JOURNAL OF PROPULSION AND POWER
Vol. 14, No. 2, March–April 1998

Overexpanded Two-Dimensional Convergent–Divergent Nozzle Performance, Effects of Three-Dimensional Flow Interactions

A. Hamed* and C. Vogiatzis†
University of Cincinnati, Cincinnati, Ohio 45221-0070

This paper presents computational results for the flowfield, surface pressure distribution, and internal thrust coefficient of a two-dimensional convergent–divergent nozzle, and compares them with existing experimental results over a range of nozzle pressure ratios (NPRs), including overexpanded conditions. The numerical simulations are based on the implicit solution of the compressible Navier–Stokes equations and the two-equation k-ω turbulence model in conservation law form and general curvilinear coordinates. The solution domain is extended laterally outside the nozzle as well as upstream and downstream of the nozzle exit to simulate the effects of external interactions. Computational results indicate that at overexpanded conditions, flow entrainment into the nozzle occurs mostly over the flaps, and that a strong secondary flow traverses the endwalls, behind the shock. Strategies for flow prediction accuracy and computational efficiency over a wide range of overexpanded NPRs are recommended, based on the assessment of computational results from both three-dimensional and two-dimensional simulations.

Introduction

RECENT efforts have focused on supersonic transport exhaust systems that meet the restrictions imposed by acoustic emission regulations and operate efficiently over a wide range of nozzle pressure ratios (NPRs) through the flight envelope. For best efficiency, the required nozzle area ratios are much higher at supersonic cruise than during subsonic acceleration.[1] The mechanical and control system constraints limit the lowest achievable area ratio, causing the two-dimensional convergent–divergent (CD) nozzle to operate overexpanded at subsonic speeds. Because it is necessary to avoid booms over inhabited areas, a 2000-lb penalty in takeoff gross weight can be associated with a 1% loss in thrust coefficient at subsonic speeds.[2] Therefore, a high degree of accuracy is required in the predictions of the thrust coefficient. However, unlike axisymmetric nozzles for rocket engines, the prediction of two-dimensional CD nozzle performance at overexpanded conditions can be very challenging, in light of the complex three-dimensional phenomena associated with shock boundary-layer interactions and flow separation over the flaps and endwalls.

Hagemann et al.[3] reported close agreement between the computed and measured postshock surface pressure in an axisymmetric nozzle at overexpanded conditions. However, the predicted shock location was much farther downstream compared to the experimental results, and would have resulted in thrust coefficient underprediction. Wilmoth and Leavitt[4] compared their two-dimensional computational results to the experimental data for the pressure distribution and thrust coefficient in a two-dimensional CD nozzle. Even at the moderate expansion area ratio of 1.3, the computations underpredicted the thrust coefficient by 0.5% at design and by 2.4% when an oblique shock was present inside the nozzle. Shieh[5] presented two-dimensional computational results for a higher-area-ratio two-dimensional CD nozzle at one overexpanded condition. His computed surface pressure distributions were not in good agreement with the experimental data of Mason et al.[6] They exhibited a much lower pressure gradient across the shock than the experiment, and unlike the experiment, the postshock surface pressure continued to rise.

Hamed and Vogiatzis[7] assessed five different turbulence models in terms of their effects on the agreement between the experimental flap centerline pressure distribution[8] and the two-dimensional computational results at overexpanded conditions. Their results indicated that both the shock location and pressure level behind the shock are affected by the turbulence model, and that the two-equation models gave the best overall agreement with the experimental data. Hamed and Vogiatzis[9] later evaluated the effects of two turbulence models on the three-dimensional flow predictions at overexpanded conditions, and determined that the computed three-dimensional effects in the surface pressure distribution are very sensitive to the turbulence models. In the three-dimensional simulations, the two equation models also gave the best overall agreement with the experimental data, even though they underpredicted the measured three-dimensional effects in the postshock flap surface pressure. Hamed and Vogiatzis[9] and Hamed et al.[10] also demonstrated that the interactions created through external flow entrainment, and their effects on the flap surface pressure distribution, might not be adequately simulated if only the nozzle interior domain is considered.

The present numerical investigation is aimed at characterizing the shock boundary-layer and external interactions, understanding the nature of the associated three-dimensional flow, and assessing different strategies for improving performance predictions in overexpanded two-dimensional CD nozzles. Different grid densities in the through-flow and lateral directions are investigated for three- and two-dimensional numerical simulations, with and without an extended external domain. Computational results are compared with experimental data for the flap surface pressure distribution and thrust coefficient over a range of NPRs, including several overexpanded conditions.[8] The results are used to evaluate the effectiveness of various computational strategies over a wide range of nozzle operating conditions.

Computational Details

Version 3.0 of the NPARC code[11] was used to obtain two- and three-dimensional numerical solutions to the Reynolds-averaged, compressible Navier–Stokes equations in strong

Received June 12, 1997; revision received Sept. 22, 1997; accepted for publication Sept. 26, 1997.

*Professor, Department of Aerospace Engineering and Engineering Mechanics, P.O. Box 210070. Fellow AIAA.

†Graduate Research Assistant, Department of Aerospace Engineering and Engineering Mechanics.

conservation law form and general curvilinear coordinates. The code uses Pulliam's diagonalized Beam–Warming central-difference time-marching scheme, with fully implicit second- and fourth-order artificial dissipation. Wilcox's k-ω turbulence model[12] was used for all the computations presented here.

Topology and Computational Grid

A multiblock grid topology was used to discretize the flowfield inside and outside the nozzle (Fig. 1). The external domain for the two-dimensional calculations extended approximately 10 nozzle exit heights h_e upstream of the nozzle exit plane and $37h_e$ downstream and in the lateral directions. For the three-dimensional calculations, the downstream and lateral extensions were limited to $20h_e$. The block topology is such that the internal flow could also be computed without the external domain. Table 1 lists the number of grid points in the individual blocks for the baseline two- and three-dimensional flow calculations. The grid points inside the nozzle constituted 61% of the total for the two-dimensional calculations and 52% for the three-dimensional calculations.

The grid for the internal flow block is presented in Fig. 2. The grid density is higher in the divergent part of the nozzle to improve the resolution of the shocks that form there. The grid is clustered near the flaps and the three-dimensional grid is also clustered for one-third of the nozzle width near the sidewall to enhance the resolution of the shear layer that forms in that region. The distance of the first point from the wall was controlled so that the maximum Y^+ at the throat centerline is 1.0 at the design pressure ratio.

Boundary Conditions

The flow was computed in one quadrant or one-half of the nozzle, depending on the dimensionality of the simulation. Symmetry boundary conditions were applied at the symmetry planes, and no-slip conditions on the nozzle walls. Stagnation conditions were specified at the nozzle inflow boundary, and static ambient pressure was specified and the rest of the primary variables were extrapolated at the downstream boundary

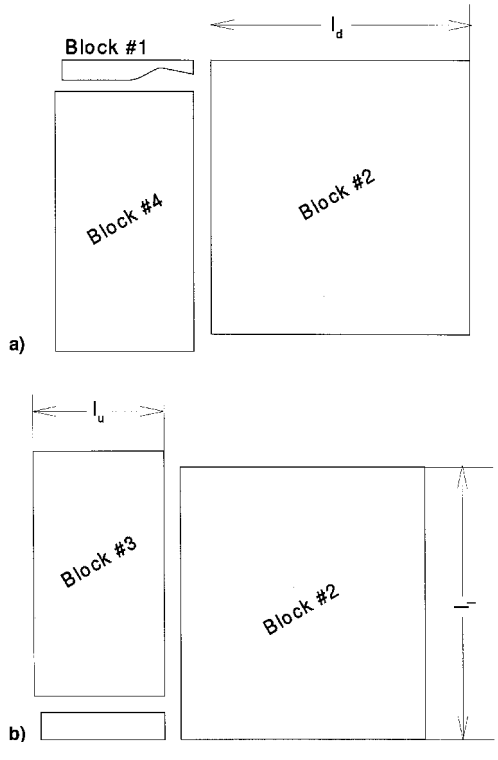

Fig. 1 a) Two-dimensional/three-dimensional grid topology on the symmetry plane betwen the sidewalls, and b) three-dimensional grid topology on the symmetry plane between the flaps.

Table 1 Grid size for typical two- and three-dimensional grids

Block no.	Two dimensional		Three dimensional	
	Dimensions	Total	Dimensions	Total
1	81 × 51	4131	81 × 51 × 71	293,301
2	31 × 81	2511	21 × 81 × 101	171,801
3	——	——	21 × 81 × 31	52,731
4	31 × 31	961	21 × 31 × 71	46,221
		7603		564,054

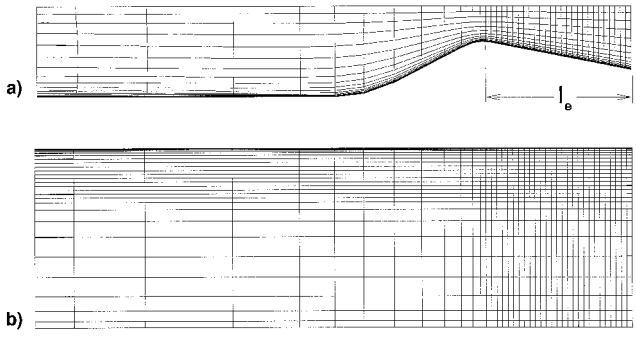

Fig. 2 Three-dimensional grid for the internal block at the symmetry plane between a) sidewalls and b) flaps.

of the external block. The contiguous boundary condition was used for all interblock boundaries.

Two types of external boundary conditions were investigated. In the first, the ambient conditions together with the smallest possible freestream Mach number were prescribed along the upstream and lateral boundaries of the external blocks. In the second, ambient pressure and temperature conditions were specified as total conditions at the external block's upstream boundary, and the primary variables were extrapolated at the lateral free boundaries. Closer agreement with the experimental thrust coefficient and flap centerline pressure distribution, in terms of shock location and strength, was obtained with the first type of boundary condition. It was also found to be associated with a more robust numerical solution behavior and, hence, was adopted in all of the two- and three-dimensional simulations. The smallest value of the freestream Mach number that would not cause stability problems ($M_\infty = 0.025$) was used for all of the cases presented here, except when otherwise stated.

Flow Initialization and Convergence

For both two- and three-dimensional simulations an internal flow solution was obtained first and used to initialize the internal/external calculation. The internal three-dimensional flowfield was initialized using an existing two-dimensional solution for the same pressure ratio and turbulence model. The internal two-dimensional solution was initialized by setting all variables equal to their nozzle inflow values. The external flow domain was introduced after advancing the internal flow solution for 2000–4000 iterations. Convergence required an additional 4000–7000 iterations, depending on the pressure ratio and the dimensionality of the problem. The Courant–Friedrichs–Lewy (CFL) number for the overexpanded cases was initially set to 1.5 and reduced to 0.8–1.0 later in the computations to avoid stability problems, and to eliminate pressure oscillations in the flowfield. A CFL number of 2.5 was used for the design pressure ratio case. The artificial viscosity levels were kept to the minimum values that would not compromise stability. The solution was found to be insensitive to the artificial dissipation levels, except for the shock crispness.

Our previous experience in two-dimensional nozzle flow simulations[7,10] indicated that the reduction of the residual receded after an initial drop of two to three orders of magnitude,

while the solution still underwent significant changes. The convergence characteristics of the three-dimensional solution exhibited a similar behavior, indicating that the residual is not an adequate measure of convergence. Therefore, the thrust was monitored, and a convergence criterion was established, requiring its variation to be smaller than 0.1% within 1000 iterations.

Results and Discussion

The computational results were obtained using the two-equation k-ω turbulence model. These results are compared with Hunter's experimental data[8] for a two-dimensional CD nozzle configuration tested under static conditions (Fig. 3). It has an area ratio of 1.8 and an aspect ratio of 2.0 at the exit plane, resulting in a design pressure ratio of 8.8. Nozzle dimensions are as follows: h_t, 1.082 in.; h_e, 1.994 in.; and w, 3.990 in.

The three-dimensional results are first presented for the surface pressure and Mach number distribution and for the endwall streamlines to demonstrate the three-dimensional shock structure and to illustrate the separation patterns and flow entrainment. The results of a grid sensitivity analysis demonstrate the effect of changing grid density ratio on the surface pressure and thrust predictions. The remainder of the results deal with the assessment of the three- and two-dimensional predictions through comparison with experimental data over a range of overexpanded conditions.

Flow Characteristics

Figures 4–6 display the salient features of the three-dimensional flowfield in the two-dimensional CD nozzle at overexpanded conditions corresponding to NPR = 2.41. The computed Mach number contours over the planes of symmetry are presented in Fig. 4. At this pressure ratio, a normal shock with

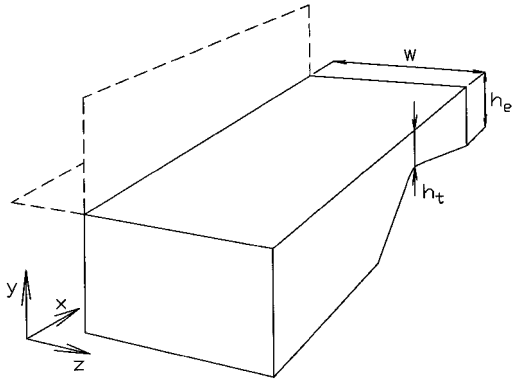

Fig. 3 One quadrant of the nozzle configuration. The symmetry planes are shown in dashed lines.

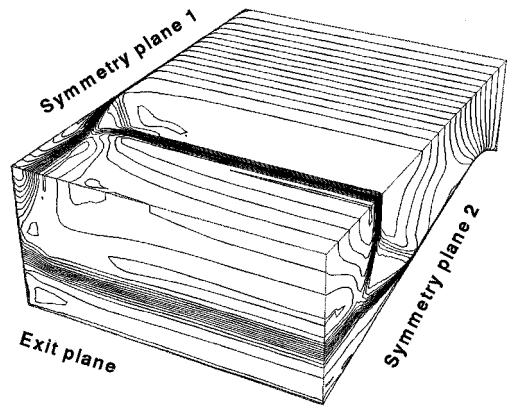

Fig. 4 Mach number contours at NPR = 2.41 (three-dimensional internal/external calculation).

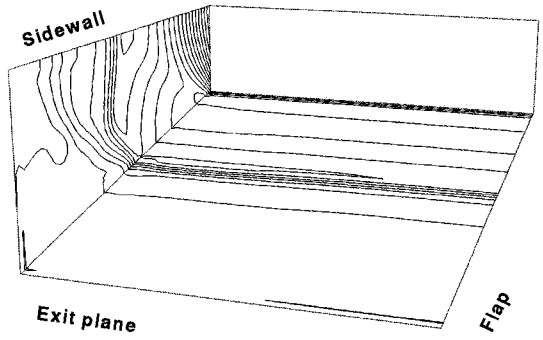

Fig. 5 Surface pressure contours at NPR = 2.41 (three-dimensional internal/external calculation).

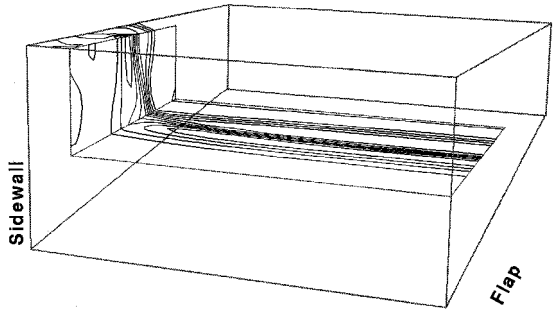

Fig. 6 Pressure contours on planes outside the shear layers at NPR = 2.41 (three-dimensional internal/external calculation).

a lambda foot can be seen on both planes. The flow separates under the front lambda foot, and a shear layer forms above the recirculating flow in the separated region. The second foot of the lambda shock does not penetrate to the flap/endwall surface but reflects at the shear layer and forms an expansion wave. The computed static pressure contours over the flap and endwall are presented in Fig. 5. One can see that the shock footprint on the endwall is strongly swept forward near the corner. On the other hand, the shock footprint over the flap is undistorted by three-dimensional effects, except for a slight backward sweep near the endwall. Figure 6, which presents the pressure contours on surfaces above the shear layers, indicates that the lambda shock feet coalesce near the corner.

The skin friction patterns at NPR = 2.41 and 1.8 are shown in Figs. 7 and 8, respectively. They clearly show a primary separation line PS_F on the flap, and a secondary attachment line SA that extends across the flap width at NPR = 2.41, and the central half at NPR = 1.8. They also show that strong three-dimensional flow effects prevail near the endwall, where one can clearly identify three lines of coalescence/divergence. PS_E denotes the primary line of separation for the incoming flow, which is similar to the shock footprint over the endwall. Behind it, the flow that is swept from the corner below the separated boundary layer forms the primary attachment line PA. Another secondary separation line SS is associated with the flow entrainment, across the flap trailing edge. The difference between the friction patterns for the two pressure ratios near the corner is caused by the different levels of external flow entrainment over the flap. The endwall figures also indicate a weaker secondary flow pattern upstream of the shock that sweeps the endwall boundary layer toward the corner and over the flap in the divergent section.

External Interactions

Figure 9 compares the two-dimensional nozzle surface pressure distribution at overexpanded conditions, computed with and without the external flow domain, with the experimental results. Closer agreement with the experimental centerline pressure distribution is observed when the external two blocks

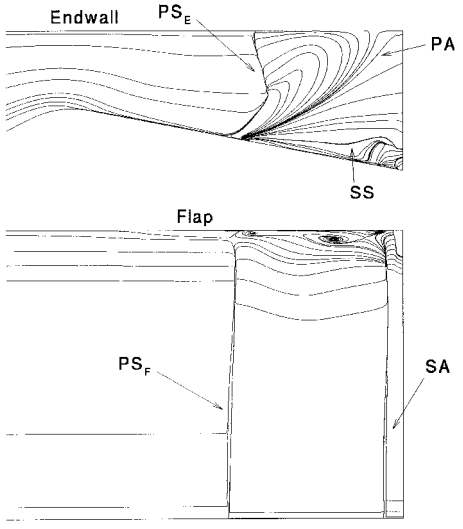

Fig. 7 Skin friction patterns at NPR = 2.41 (three-dimensional internal/external calculation).

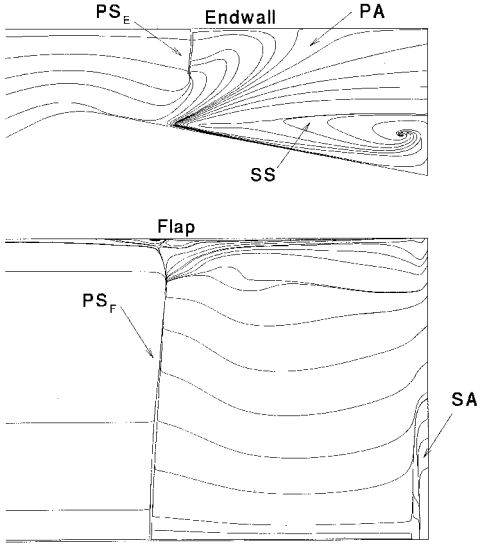

Fig. 8 Skin friction patterns at NPR = 1.80 (three-dimensional internal/external calculation).

are included in the solution domain to simulate freestream interactions. Restricting the computations to the nozzle's internal domain results in overpredicting the nozzle flap surface pressure behind the shock.

The three-dimensional computational results for the flap surface pressure distribution are presented in Fig. 10 and are compared with the two-dimensional computational results with external domain and to Hunter's experimental data.[8] One can see a noticeable improvement in the predicted shock location at the flap centerline with the three-dimensional simulations, which also reasonably reproduce the experimentally reported difference in the shock location near the endwall and at the centerline. However, the pressure rise across the shock near the endwall and, consequently, the thrust, are slightly overpredicted. The turbulence model performance in the flow regions dominated by strong pressure gradients and complex three-dimensional secondary flows is the most likely culprit for this discrepancy.[13] This is confirmed by the results we obtained with the Spalart–Allmaras turbulence model,[9] where the postshock flap surface pressure near the endwall was underpredicted. However, that model also resulted in unrealistically high total pressures near the corner.

Increasing the specified external freestream Mach number caused the shock to shift downstream and resulted in lower

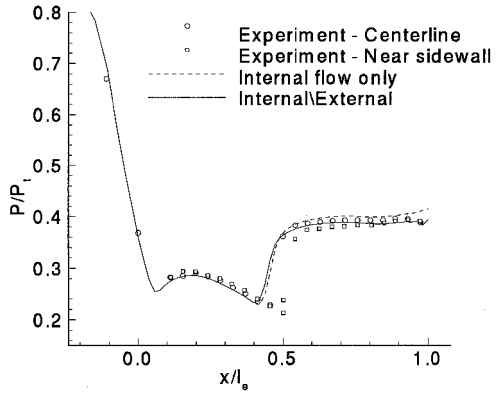

Fig. 9 Surface pressure distributions at NPR = 2.41 for two different two-dimensional computational domains.

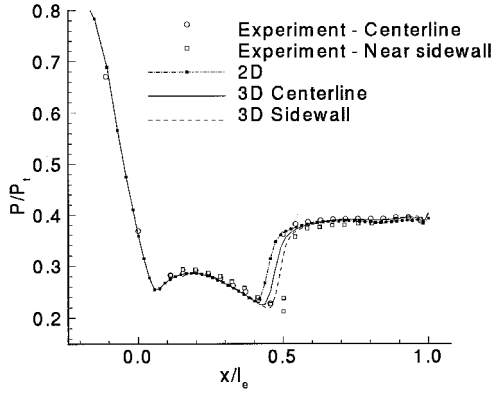

Fig. 10 Three-dimensional effects on the surface pressure distributions at NPR = 2.41 (internal/external calculation).

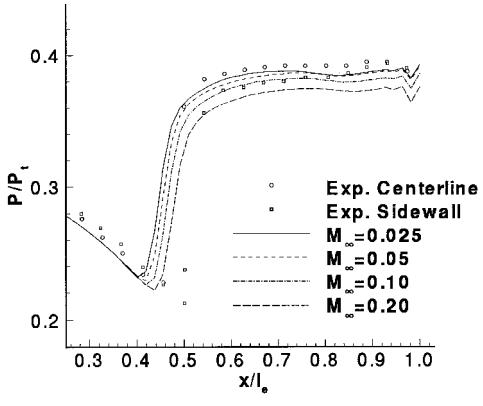

Fig. 11 Effect of M_∞ on the surface pressure distribution at NPR = 2.41 (two-dimensional internal/external calculation).

postshock static pressure (Fig. 11). The combined effects improved the agreement between the computed and experimentally measured static thrust as the freestream Mach number was increased. The linear decline in the predicted thrust coefficient with increased freestream Mach number is shown in Fig. 12. These results were used to adjust (augment) the computed thrust to the $0.025M_\infty$ equivalent value, whenever it was necessary to specify a freestream Mach number greater than 0.025 for stability.

Grid Sensitivity Analysis

An extensive study was conducted to investigate the sensitivity of the computed thrust coefficient and surface pressure distribution to the level of grid refinement in the through-flow and lateral directions independently. All calculations were performed at NPR = 2.41 using the k-ω turbulence model. Figure

Table 2 Grid density ratio effect on thrust[a]

Internal only			
J_{max}	K_{max}	C_F	Error, %
81	51	0.9219	1.8
121	51	0.9238	2.0
121	101	0.9192	1.5
241	102	0.9189	1.5

[a]Obtained with two-dimensional internal-only calculations.

Table 3 Lateral grid density effect on thrust[a]

Internal + external			
J_{max}	K_{max}	C_F	Error, %
121	51	0.9187	1.5
121	101	0.9188	1.5
121	201	0.9180	1.4

[a]Obtained with two-dimensional internal/external calculations.

Table 4 Grid density effect on thrust[a]

J_{max}	K_{max}	L_{max}	C_F	Error, %
81	51	71	0.9107	0.7
102	64	89	0.9146	1.1

[a]Obtained with three-dimensional internal/external calculations.

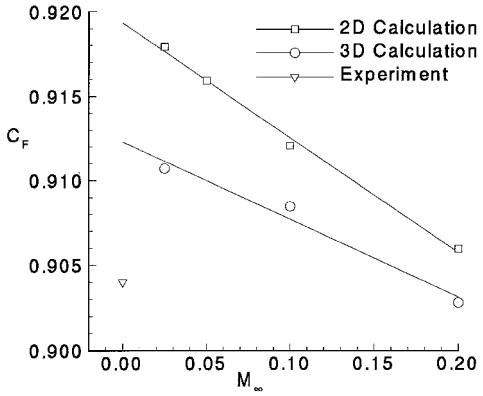

Fig. 12 Effect of M_∞ on the thrust predictions at NPR = 2.41 (internal/external calculations).

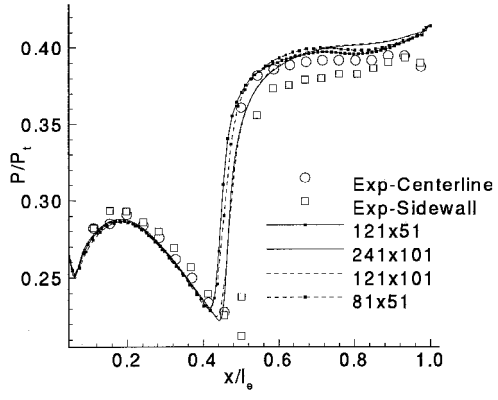

Fig. 13 Effect of grid density ratio on the surface pressure at NPR = 2.41 (two-dimensional internal domain).

13 presents the results for the surface pressure. Table 2 summarizes the predicted thrust sensitivity to the grid for two-dimensional simulations in the internal nozzle domain only. The predicted shock location and postshock pressure are both sensitive to the number of grid points in the lateral direction (Fig. 13). The surface pressure distributions also indicate that 121 points in the streamwise direction are sufficient for grid independence, when the lateral grid resolves the sharp velocity gradients across the shear layer.

The results of a similar analysis for internal/external flow calculations are presented in Table 3 for the thrust and in Fig. 14 for the corresponding surface pressure distributions. One

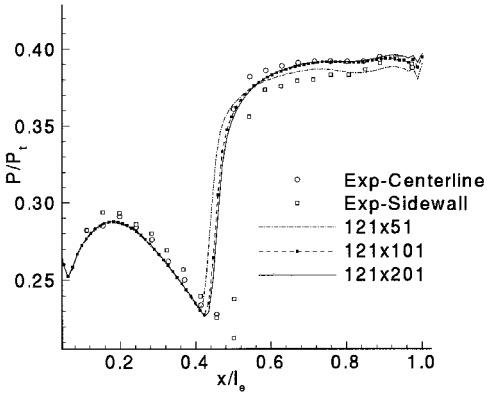

Fig. 14 Effect of lateral grid size on the surface pressure at NPR = 2.41 (two-dimensional internal/external domain).

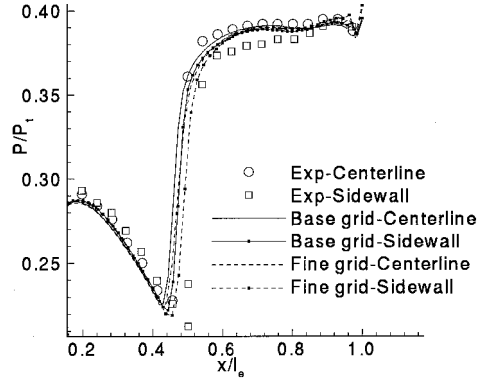

Fig. 15 Effect of grid density on the surface pressure at NPR = 2.41 (two-dimensional internal/external domain).

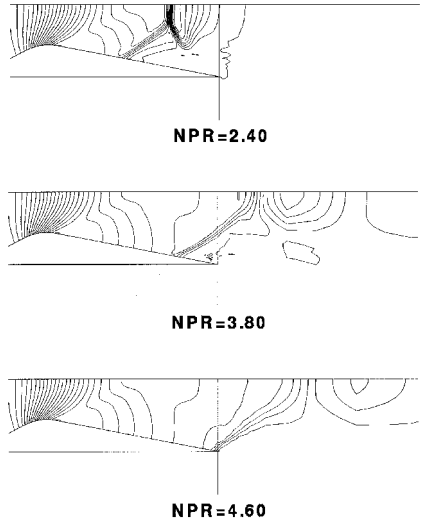

Fig. 16 Pressure contours showing the effect of NPR on the shock structure (two-dimensional internal/external calculations).

Table 5 Thrust predictions and difference from experimental results

NPR	Experiment	Two-dimensional, 81 × 51		Three-dimensional, 81 × 51 × 71
		Internal	Internal + external	Internal + external
1.8	0.831	0.9110	0.9069	0.8858
		(8.0%)	(7.6%)	(5.5%)
2.4	0.904	0.9219	0.9179	0.9107
		(1.8%)	(1.4%)	(0.7%)
2.6	0.912	——	0.9275[a]	——
		——	(1.6%)[a]	——
3.0	0.923	0.9497	0.9445[a]	——
		(2.7%)	(2.1%)[a]	——
3.4	0.935	0.9523	0.9506[a]	0.9449[a]
		(1.7%)	(1.6%)[a]	(1.0%)[a]
3.8	0.942	0.9570	0.9573[a]	——
		(1.5%)	(1.5%)[a]	——
4.6	0.959	0.9660	0.9619	——
		(0.7%)	(0.3%)	——
5.0	0.964	0.9710	0.9695	——
		(0.7%)	(0.5%)	——
6.2	0.978	0.9832	0.9839	——
		(0.5%)	(0.6%)	——
7.0	0.983	0.9878	0.9879	——
		(0.5%)	(0.5%)	——
8.0	0.987	0.9905	0.9905	——
		(0.3%)	(0.4%)	——
8.8	0.987	0.9913	——	0.9896[b]
		(0.4%)	——	(0.3%)[b]

[a]Results obtained with M_{inf} = 0.2 and corrected using data of Fig. 12.
[b]Internal flow only.

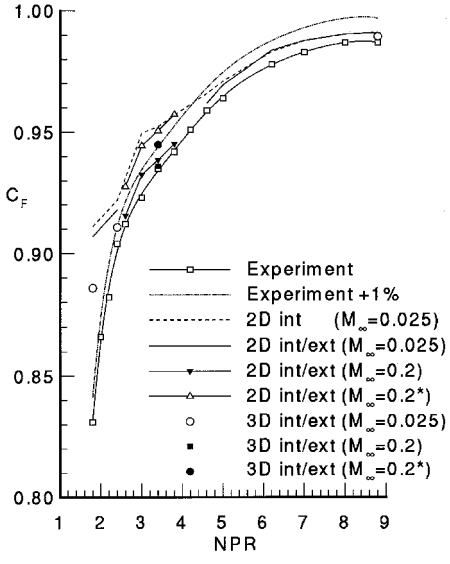

Fig. 17 Comparison of two- and three-dimensional thrust predictions with experimental data.

can observe that thrust predictions are less sensitive to the lateral grid size, when the external flow is included in the solution domain. Grid-independent performance predictions can be obtained in this case with a 121 × 51 internal grid (8400 total internal and external points) compared with a 121 × 201 grid (24,000 points) for internal domain only.

The total number of grid points was doubled to conduct a three-dimensional grid sensitivity analysis. The resulting numerical thrust overprediction was higher compared with the baseline case (Table 4), yet the surface pressure distribution showed closer agreement to the experimentally observed shock location (Fig. 15). Although some grid dependency seems to remain in the presented three-dimensional calculations, it is within the error bounds of the experimental data.

Thrust Predictions

Some of the predicted two-dimensional pressure contours are shown in Fig. 16 to relate the evolution of the shock structure to the thrust predictions accuracy at various NPRs. The predicted thrust coefficients for various computational domains (two-dimensional/three-dimensional, internal/internal–external) are compared with the experimental values in Table 5 and Fig. 17 over the range of tested NPRs. The results indicate that the two-dimensional calculations with external domain overpredict the thrust by less than 0.5% for NPRs greater than 3.8. The difference between the internal-only and internal/external two-dimensional calculations is less than 0.2% for NPRs greater than 4.6, where the shock structure is outside the nozzle. The three-dimensional thrust predictions, on the other hand, are within 0.7% of the experimental results, even at NPR = 2.4, with the normal and lambda shock structure well within the nozzle. However at lowest NPR of 1.8, the thrust predictions exceed the experimental values by 5.5 and 7.6%, respectively, for three- and two-dimensional simulations. Note that, because a choke plate is used upstream of the test section, the experimental upstream conditions, and especially the total pressure profile, are not precisely known. This uncertainty is expected to account for some of the variation between the computed results and the experimental measurements.

Conclusions

Two- and three-dimensional flow computations were performed in a two-dimensional CD nozzle for NPRs ranging from design to severely overexpanded, using different computational domains. The three-dimensional results reveal a complex shock structure and extensive flow separation over the flaps at overexpanded conditions. Pronounced three-dimensional effects were predicted over the endwall and near the flap corner, especially at low NPRs. They include complex primary separation and reattachments lines over the endwall, and a secondary pair associated with flow entrainment over the flap. Decreasing the NPR increases flow entrainment and alters the locations of the primary separation and secondary reattachment lines over the flap.

The grid refinement study revealed that both shock location and postshock surface pressure are very sensitive to grid refinement in the lateral direction, especially in internal-flow-only simulations. The inclusion of external blocks in the solution domain is essential to simulate the effects of freestream interactions. In addition to being more economical computationally, because the total number of grid points required is smaller, the resulting surface pressure predictions are in closer agreement with the experimental values. The three-dimensional simulations further improve the agreement between the computed shock location and the postshock pressure at the flap centerline. They agree well with the experimental data for the shock location, but slightly overpredict the postshock pressure near the endwall. Even though strong three-dimensional effects are predicted near the corner, these effects are not reflected in the flap surface pressure.

The thrust predictions are generally higher than the experiment, but agreement with the experimental results varies significantly with the NPR. The two-dimensional thrust predictions with the external domain agree with the measurements within experimental uncertainty for moderate pressure ratios, before the shocks move far enough into the nozzle to cause extensive flow separation over the flaps. The three-dimensional flow simulations can extend the agreement with the experimental values when normal shocks and strong crossflows are present inside the nozzles, but require 50 times the computational resources. However, the turbulence model still limits the ability to reproduce the postshock experimental pressure near the corner at the lowest pressure ratios. Finally, the specified uniform upstream conditions are likely to be a cause of variation between the computed results and the experimental mea-

surements. This effect cannot be determined in the absence of experimental upstream conditions, but might be assessed through a sensitivity study of the influence of varying the upstream total pressure profile.

Acknowledgments

This work was sponsored by General Electric Aircraft Engines Contract 200-1Q-14C43820. Kevin Early was the Contract Monitor. The computational work was performed on the Cray Y-MP of the Ohio Supercomputer Center.

References

[1]Dusa, D. J., "Exhaust Nozzle System Design Considerations for Turboramjet Propulsion Systems," *Proceedings of the 10th International Symposium on Airbreathing Engines*, edited by Frederick S. Billig, Vol. 2, AIAA, Reston, VA, 1991, pp. 1100–1110.

[2]Gikley, S. C., Hines, R. H., and Shaw, R. J., "Installing a Propulsion System in the HSCT," *Mechanical Engineering*, Vol. 117, No. 8, 1995, pp. 98–101.

[3]Hagemann, G., Schley, C.-A., Odintsov, E., and Sobatchkine, A., "Nozzle Flowfield Analysis with Particular Regard to 3D-Plug-Cluster Configurations," AIAA Paper 96-2954, July 1996.

[4]Wilmoth, R. G., and Leavitt, L. D., "Navier-Stokes Predictions of Multifunction Nozzle Flows," *Society of Automotive Engineers Transactions*, Vol. 96 Sec. 6, Paper 871753, 1987, pp. 6.865–6.879.

[5]Shieh, F. S., "Navier-Stokes Solutions of the Transonic Nozzle Flow with Shock Induced Flow Separations," *Journal of Propulsion and Power*, Vol. 8, No. 4, 1992, pp. 829–835.

[6]Mason, M. L., Putnam, L. E., and Re, R. J., "The Effect of Throat Contouring on Two-Dimensional Converging-Diverging Nozzles at Static Conditions," NASA TP-1704, Aug. 1980.

[7]Hamed, A., and Vogiatzis, C., "Assessment of Turbulence Models in Overexpanded 2D-CD Nozzles," *Journal of Propulsion and Power*, Vol. 13, No. 3, 1996, pp. 444–445.

[8]Hunter, C. A., "An Experimental Analysis of Passive Shock Boundary Layer Interaction Control for Improving the Off-Design Performance of Jet Exhaust Nozzles," M.S. Thesis, George Washington Univ., Washington, DC, Sept. 1993.

[9]Hamed, A., and Vogiatzis, C., "Three-Dimensional Flow Computations and Thrust Predictions in 2DCD Overexpanded Nozzles," AIAA Paper 97-0030, Jan. 1997.

[10]Hamed, A., Vogiatzis, C., and Yeuan, J. J., "Performance Prediction of Overexpanded 2DCD Nozzles," *Proceedings of the 12th International Symposium on Air Breathing Engines*, Vol. 1, AIAA, Reston, VA, 1995, pp. 447–459.

[11]"NPARC User's Guide: Version 3.0," The NPARC Alliance, Sept. 1996.

[12]Yoder, D. A., Georgiadis, N. J., and Orkwis, P. D., "Implementation of a Two Equation k-ω Turbulence Model in NPARC," NASA TM-107080, Jan. 1996.

[13]Bradshaw, P., "Progress in Turbulence Research," AIAA Paper 90-1480, June 1990.